Acta Cryst. (1960). **13**, 349

The Energy Flow of X-rays in an Ideally Perfect Crystal: Comparison Between Theory and Experiments

By Norio Kato

Division of Engineering and Applied Physics, Harvard University, Cambridge 38, *Massachusetts, U.S.A.*

(*Received* 15 *July* 1959)

A theory of X-ray energy flow in an ideally perfect crystal is developed based upon the ordinary dynamical theory of diffraction in a more practical form. The following topics are discussed: the spatial intensity profile of a reflected and transmitted beam, and L. C. Brown's experiments on the behavior of a transmitted beam which satisfies the Bragg condition. (Thesis, Florida State University, 1952). Agreement between theory and experiment is fairly good. It is pointed out that an intensity enhancement at the margins of a diffracted beam can be explained in terms of a diffraction effect.

1. Introduction

In order to understand the diffraction phenomena of X-ray waves in ideally perfect crystals we have to consider the behavior of energy flow in such crystals. Several experiments (Cork, 1932; Murdock, 1934; Borrmann, 1950; Borrmann *et al.*, 1955) show that X-ray energy flows mainly in a direction parallel to the reflecting net plane, in sufficiently thick crystals. Theoretical studies (Kato, 1952; v. Laue, 1952, 1953; Niehrs, 1956; Kato, 1958; Ewald, 1958; Wagner, 1959) also have been carried out on this problem and the above experimental results have been explained qualitatively. It seems, however, that the theories presented hitherto have been concerned mainly with fundamentals and have not been developed in a form convenient to compare with experimental data. In addition some interesting experiments recently reported have not yet received a proper explanation. In this paper the author presents a more detailed theory of the energy flow in ideally perfect crystals and compares it with the available experimental results. A detailed discussion is given of the spatial intensity profiles of the diffracted and the transmitted beam, i.e. the intensity profiles of cross-sections of these beams. Also discussed are the experiments of L. C. Brown (1952) on the lateral displacement of the transmitted beam and on rocking curves of a selected part of the transmitted beam.

This paper does not consider 'Pendellösung' interference phenomena at all. Actually, the 'hook-shaped' fringes reported by Kato & Lang (1959) show that the ordinary theories should be modified to some extent. The present theory is unsatisfactory for understanding such diffraction phenomena. Nevertheless it seems worth-while to present the theory in this form because a simple treatment described here may be applied to some problems in which we are concerned only with an intensity averaged over a 'Pendellösung' period. In addition, the present theory will serve for comparing the usual theories with a revised theory which will be presented in the near future (Kato, in preparation).

2. Transmission power and reflection power

(A) *General considerations*

According to the dynamical theory of diffraction, four plane waves are produced in a crystal when an incident wave satisfies the Bragg condition for a particular net plane. Their wave vectors may be written $\mathbf{D}^{(1)}\mathbf{O}$, $\mathbf{D}^{(2)}\mathbf{O}$, $\mathbf{D}^{(1)}\mathbf{G}$ and $\mathbf{D}^{(2)}\mathbf{G}$. Here $D^{(1)}$ and $D^{(2)}$ are dispersion points (wave points), each of which corresponds to one of the branches of the dispersion surface (cf. Fig. 1). O and G are the origin and a lattice point of the reciprocal lattice respectively. The former two vectors correspond to a transmitted beam and the latter two correspond to a reflected beam.

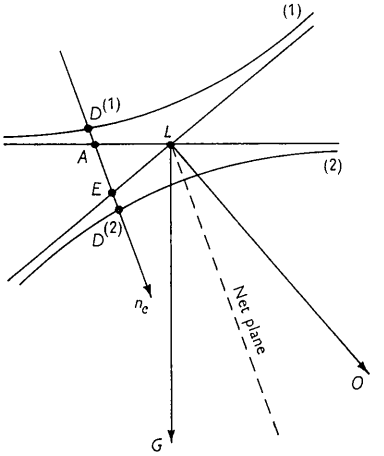

Fig. 1. Dispersion points and dispersion surface.

As to the energy flow, the $\mathbf{D}^{(1)}\mathbf{O}$-wave and $\mathbf{D}^{(1)}\mathbf{G}$-wave combine together and go through the crystal in a particular direction. This direction is the normal of

the dispersion surface at $D^{(1)}$. In the same way the $\mathbf{D}^{(2)}\mathbf{O}$-wave and $\mathbf{D}^{(2)}\mathbf{G}$-wave combine and go through the crystal in the direction of the normal at $D^{(2)}$.

The points $D^{(1)}$ and $D^{(2)}$ are determined by boundary conditions at the entrance surface and by the angular deviation of the incident beam from the Bragg angle, i.e. 'Anregungsfehler.' This may be easily understood through the following geometrical construction. In Fig. 1, L is a point on the Laue circle, i.e. on the intersection of two spheres of radius $K=2\pi/\lambda$ ($\lambda=$ wavelength) drawn with O and G as their centers, respectively.* E is the wave-point of the incident beam and therefore the angle EOL measures the angular deviation from the precise Bragg condition. If the crystal surface is sufficiently large, the tangential component of the wave vector of the incident plane wave must be equal to that of the induced crystal waves. Therefore the dispersion points $D^{(1)}$ and $D^{(2)}$ are determined by the intersection of the dispersion surface with a line parallel to $\mathbf{n}_e$ passing through E, where $\mathbf{n}_e$ is a unit vector normal to the incident surface.

If we change the glancing angle from a sufficiently small angle to a sufficiently large angle, the direction of the energy flow of the $\mathbf{D}^{(1)}\mathbf{O}$- and $\mathbf{D}^{(1)}\mathbf{G}$-waves changes from the direction of $\mathbf{K}_0$ to that of $\mathbf{K}_g$, and the direction of energy flow of the $\mathbf{D}^{(2)}\mathbf{O}$- and $\mathbf{D}^{(2)}\mathbf{G}$-waves changes from $\mathbf{K}_g$ to $\mathbf{K}_0$. Here $\mathbf{K}_0$ is the wave vector of an incident beam which satisfies the Bragg condition precisely and $\mathbf{K}_g$ is $\mathbf{K}_0+2\pi\mathbf{g}$, ($\mathbf{g}=\mathbf{OG}$).

After arriving at the back surface of the crystal each energy flow splits into a diffracted beam and a transmitted beam which travel outside the crystal. The wave points of the external beams are A and E respectively if we assume a parallel-sided crystal slab.* Therefore two parallel beams emerge from the crystal in the direction of **EO** and two also in the direction of **AG**, these directions corresponding to those of the transmitted and diffracted beams, respectively. Fig. 2 shows the situation.

(B) *Theory*

According to Laue's treatment (1952), the Poynting vector in ideally perfect crystals can be expressed simply if it is averaged over time and over a space covering a region larger than a period of 'Pendellösung' interference. His result is as follows:

$$\mathbf{S}^{(i)}=\mathbf{k}_0^{(i)}|D_0^{(i)}|^2+\mathbf{k}_g^{(i)}|D_g^{(i)}|^2, \quad (i=1 \text{ and } 2) \tag{1}$$

where $\mathbf{S}^{(i)}$ is an averaged Poynting vector, $\mathbf{k}_0^{(i)}$ and $\mathbf{k}_g^{(i)}$ are the wave vector of a transmission and reflection wave in the crystal, respectively, and $D_0^{(i)}$ and $D_g^{(i)}$ are their amplitudes. The vectors $\mathbf{k}_0^{(i)}$ and $\mathbf{k}_g^{(i)}$ are equal to $\mathbf{K}_0$ and $\mathbf{K}_g$, to a sufficiently good approximation, so long as we are concerned with the Poynting vector. The amplitudes $|D_0^{(i)}|^2$ and $|D_g^{(i)}|^2$ are calculated from the ordinary theory as follows:

$$\left.\begin{aligned}
|D_0^{(1)}|^2 &= \frac{1+2y^2+2y(1+y^2)^{\frac{1}{2}}}{4(1+y^2)} \\
&\quad\times \exp\left[-\mu_0 t+2A(\chi+yg)/(1+y^2)^{\frac{1}{2}}\right] \\
|D_0^{(2)}|^2 &= \frac{1+2y^2-2y(1+y^2)^{\frac{1}{2}}}{4(1+y^2)} \\
&\quad\times \exp\left[-\mu_0 t-2A(\chi+yg)/(1+y^2)^{\frac{1}{2}}\right] \\
|D_g^{(1)}|^2 &= \frac{b}{4(1+y^2)} \\
&\quad\times \exp\left[-\mu_0 t+2A(\chi+yg)/(1+y^2)^{\frac{1}{2}}\right] \\
|D_g^{(2)}|^2 &= \frac{b}{4(1+y^2)} \\
&\quad\times \exp\left[-\mu_0 t-2A(\chi+yg)/(1+y^2)^{\frac{1}{2}}\right].
\end{aligned}\right\} \tag{2}$$

Here the notation is the same as that used in Zachariasen (1945) by which b is very nearly the ratio of the direction cosines of the incident and diffracted waves (Zach. [3·115]) and y is the 'Anregungsfehler' (defined by Zach. [3·114b], [3·123] and [3·141]). For convenience we introduce a parameter

$$x=y/(1+y^2)^{\frac{1}{2}}. \tag{3}$$

If we define the transmission power $P_0^{(i)}$ by the ratio of the transmitted energy of the (i)-wave to the energy of the incident wave, and the reflection power $P_g^{(i)}$ by the ratio of the reflected energy of the (i)-wave to the incident energy, they may be written as follows:

$$\left.\begin{aligned}
P_0^{(1)} &= \frac{G_0}{4}(1+x)^2 \\
&\quad\times \exp\left[-\mu_0 t+2A\chi(1-x^2)^{\frac{1}{2}}+2Agx\right] \\
P_0^{(2)} &= \frac{G_0}{4}(1-x)^2 \\
&\quad\times \exp\left[-\mu_0 t-2A\chi(1-x^2)^{\frac{1}{2}}-2Agx\right] \\
P_g^{(1)} &= \frac{bG_g}{4}(1-x^2) \\
&\quad\times \exp\left[-\mu_0 t+2A\chi(1-x^2)^{\frac{1}{2}}+2Agx\right] \\
P_g^{(2)} &= \frac{bG_g}{4}(1-x^2) \\
&\quad\times \exp\left[-\mu_0 t-2A\chi(1-x^2)^{\frac{1}{2}}-2Agx\right],
\end{aligned}\right\} \tag{4}$$

where G_0 and G_g are geometrical factors arising from change of the beam width. They are written as follows:

$$\left.\begin{aligned}
G_0 &= \frac{\cos(\mathbf{s}.\mathbf{n}_e)}{\cos(\mathbf{k}_0.\mathbf{n}_e)}\cdot\frac{\cos(\mathbf{k}_0.\mathbf{n}_a)}{\cos(\mathbf{s}.\mathbf{n}_a)} \\
G_g &= \frac{\cos(\mathbf{s}.\mathbf{n}_e)}{\cos(\mathbf{k}_0.\mathbf{n}_e)}\cdot\frac{\cos(\mathbf{k}_g.\mathbf{n}_a)}{\cos(\mathbf{s}.\mathbf{n}_a)}
\end{aligned}\right\} \tag{4'}$$

* For simplicity we neglect the effect of the mean value of polarizability, in the X-ray case, or of inner potential, in the electron case. The more general situation is described in Fig. 1 of the author's earlier paper (*J. Phys. Soc. Jap.* 7 (1952) 397). Also, we consider the incident X-rays to be plane-polarized.

where $\mathbf{n}_a$ is the unit vector of the normal of the exit surface.

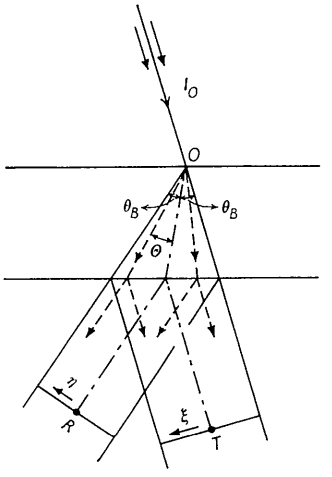

Fig. 2. Diffracted beam (R) and transmitted beam (T) due to a single crystal.

In Fig. 2, we consider an angle Θ between a direction $\mathbf{S}^{(i)}$ and the net plane concerned. From equation (1) this may be expressed as follows,

$$\tan\Theta = \frac{|D_g^{(i)}|^2 - |D_0^{(i)}|^2}{|D_g^{(i)}|^2 + |D_0^{(i)}|^2}\tan\theta_B\,. \tag{5}$$

Therefore, if we introduce a geometrical parameter

$$p = \tan\Theta/\tan\theta_B\,, \tag{6}$$

the relations between x and p are

$$\left.\begin{aligned} p &= \frac{b(1-x)-(1+x)}{b(1-x)+(1+x)} \quad \text{for the (1)-wave} \\ \text{and}\quad p &= \frac{b(1+x)-(1-x)}{b(1+x)+(1-x)} \quad \text{for the (2)-wave}\,. \end{aligned}\right\} \tag{7}$$

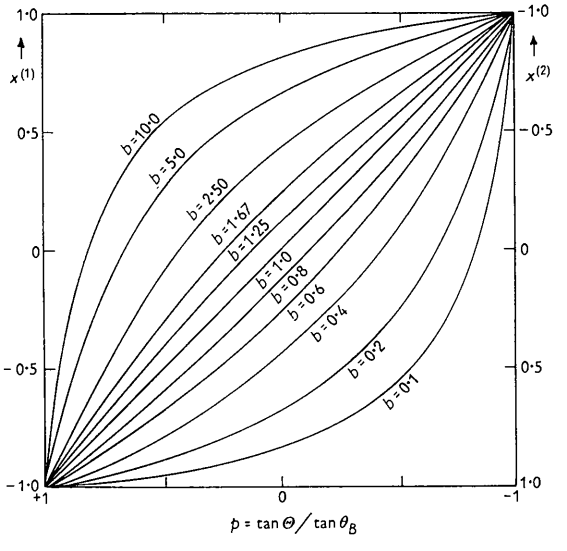

Fig. 3. Relation between x and p.

If b is nearly equal to 1,

$$\left.\begin{aligned} x &= -p+\tfrac{1}{2}(1-p^2)c \quad \text{for the (1)-wave} \\ \text{and}\quad x &= p+\tfrac{1}{2}(1-p^2)c \quad \text{for the (2)-wave}\,, \end{aligned}\right\} \tag{7'}$$

where

$$c = b-1, \quad |c| \ll 1\,. \tag{8}$$

In the symmetrical Laue case, i.e. $b=1$, it is clear that $x=\pm p$, and $P_0^{(i)}$ and $P_g^{(i)}$ can be expressed in terms of the parameter p instead of x in equation (4). Relations between x and p in general cases are shown in Fig. 3.

3. Spatial intensity profiles of the transmitted and reflected beam

(A) *Theoretical spatial intensity profiles*

As explained in § 2(A), if an incident beam were ideally parallel and monochromatized and also its cross section small enough, we might be able to observe separately two transmitted beams and two reflected beams. Actually, it is not easy to obtain such an incident beam with sufficient intensity, so that no experimental evidence of such a separation has yet been obtained. Here, however, we consider the more feasible experimental condition that the incident beam has an angular width of some extent but is sufficiently narrow in cross section. Under this condition, various plane waves occur in the crystal simultaneously. We assume that there is no phase relation between them. We have a transmitted and diffracted beam of a definite width as shown in Fig. 2.

The intensity distribution along the axes of the coordinates ξ and η in Fig. 2 can be expressed as follows:

$$\left.\begin{aligned} I_0(\xi) &= \frac{\delta E_0}{\delta\xi} = \frac{\delta E_0}{\delta y}\cdot\frac{dy}{dx}\cdot\frac{dx}{dp}\cdot\frac{\delta p}{\delta\xi} \\ I_g(\eta) &= \frac{\delta E_g}{\delta\eta} = \frac{\delta E_g}{\delta y}\cdot\frac{dy}{dx}\cdot\frac{dx}{dp}\cdot\frac{\delta p}{\delta\eta}\,, \end{aligned}\right\} \tag{9}$$

where δE_0 and δE_g are the total energies of a transmitted and a reflected beam which pass through an interval $\delta\xi$ and $\delta\eta$ respectively.

$I_0(\xi)$ (and $I_g(\eta)$) are each composed of two waves, (1) and (2), which are produced by incident beams having different angles of incidence. Equation (7) shows, however, that the relations between x and p for wave (2) can be obtained from those for wave (1) just by changing the sign of x, and vice versa. Therefore, if we denote the energy of an incident beam in the angular range from y to $y+\delta y$ as $I_e(y)\delta y$,

$$I_0(\xi) = \{I_e(y)P_0^{(1)}(x) + I_e(-y)P_0^{(2)}(-x)\}\left(\frac{dy}{dx}\right)\left|\frac{dx}{dp}\right|\left(\frac{\delta p}{\delta\xi}\right) \tag{10}$$

$$I_g(\eta) = \{I_e(y)P_g^{(1)}(x) + I_e(-y)P_g^{(2)}(-x)\}\left(\frac{dy}{dx}\right)\left|\frac{dx}{dp}\right|\left(\frac{\delta p}{\delta\eta}\right), \tag{11}$$

where y and x are the values corresponding to a value of the geometrical parameter p of the wave (1) according to equations (3) and (7). From equation (3), dy/dx is easily obtained. If we notice the general situation that a direction of energy flow $\mathbf{S}^{(i)}$ is perpendicular to the dispersion surface, we can obtain

$$\left|\frac{dx}{dp}\right|\left(\frac{\delta p}{\delta \xi}\right) \quad \text{and} \quad \left|\frac{dx}{dp}\right|\left(\frac{\delta p}{\delta \eta}\right)$$

in a simple form as shown in Appendix B.

Thus we can obtain all other factors in equation (10) except for the unknown quantity $I_e(y)$. To obtain a theoretical intensity profile we have to make some assumptions about the intensity distribution of the incident beam. Actually the Bragg relation is satisfied only when the deviation of the incident beam from the Bragg angle is less than several seconds of arc at most. Since this angular range is very small, it is reasonable to assume that

$$\begin{aligned} I_e(y) &= I_e(\text{const.}) \quad |y| < y_0 \\ &= 0 \qquad\qquad\quad |y| > y_0 , \end{aligned} \tag{12}$$

where y_0 is a constant corresponding to the angular width of the incident beam. Using this assumption equation (9) becomes, in the symmetrical Laue case for a parallel-sided crystal of thickness t_0,

$$\left.\begin{aligned} I_0(p) &= \frac{I_e}{2\,t_0 \sin\theta_B}\,\frac{1-p}{(1-p^2)^{\frac{1}{2}}(1+p)} \\ &\quad \times \cosh 2A\chi(1-p^2)^{\frac{1}{2}} \exp -\mu_0 t_0 \\ I_g(p) &= \frac{I_e}{2\,t_0 \sin\theta_B}\,\frac{1}{(1-p^2)^{\frac{1}{2}}} \\ &\quad \times \cosh 2A\chi(1-p^2)^{\frac{1}{2}} \exp -\mu_0 t_0 . \end{aligned}\right\} \tag{13}$$

In the general case we may not be able to use the assumption (12). If we consider the ratio I_g/I_0, however, we can always eliminate an arbitrary form of the function $I_e(y)$. From equations (4), (10), (11) and (B8a, b),

$$\frac{I_g}{I_0} = \frac{\cos(\mathbf{k}_0\mathbf{n}_a)}{\cos(\mathbf{k}_g\mathbf{n}_a)}\,\frac{1-x}{1+x} = \frac{1}{b}\,\frac{\cos(\mathbf{k}_0\mathbf{n}_a)}{\cos(\mathbf{k}_g\mathbf{n}_a)}\,\frac{1+p}{1-p}. \tag{14}$$

This result is quite general and does not depend upon absorption, net plane, and the intensity distribution of the incident beam.

(B) *Comparison between theory and experiment*

Fig. 4 shows examples of theoretical spatial intensity profiles according to equation (13). In the diffraction beam the intensity increases at the margins of the profile in the case of thin crystals. This may seem curious at first sight because the X-rays flow in the direction of $p \simeq 0$ when the Bragg condition is satisfied exactly. It is, however, understandable if we consider the fact that changes of p due to angular changes of the incident beam are so rapid in the vicinity of $p \simeq 0$ (cf. equation (3)) that most of the energy of the incident beam flows in directions close to the margins of the profile.* In a transmission beam, however, the intensity decreases in a monotonic way as one approaches the margin nearer to the diffracted beam, in the thin crystal case.

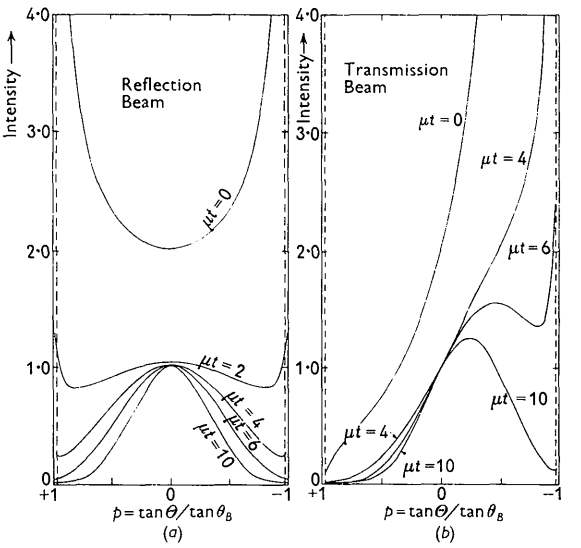

Fig. 4. Theoretical spatial intensity profiles of a reflection beam (a) and a transmission beam (b), in the symmetrical Laue case.

In thicker crystals the intensity at the margins decreases markedly for both diffracted and transmitted beams but the central part does not decrease by more than half the value for a non-absorbing crystal. This is essentially due to the Borrmann effect.

These theoretical predictions agree fairly well with experimental results. Fig. 7 of the previous paper (Kato & Lang, 1959) shows a pair of section patterns due to a diffracted beam and a transmitted beam.† We observe a high intensity at the margins of the diffracted beam in the thin part of the crystal and also a decrease of the margin intensity as crystal thickness increases.

It seems worth-while here to mention an observed intensity enhancement at the margins of a diffracted beam in the case of neutron diffraction (Knowles, 1956). In his case the specimen (calcite) might have been almost perfect because the Borrmann effect was observed strongly by using X-ray diffraction. Therefore his observations may probably be explained by the margin effect described above.

In fact, this kind of observation in X-ray Laue photographs has been reported already by a few authors

* This situation was pointed out by Borrmann *et al.* (1955) qualitatively. They did not predict, however, an actual intensity enhancement at the margins: their calculations were mainly concerned with thick crystals.

† Here we are concerned only with averaged intensity distributions taken over 'Pendellösung' fringes.

(Cork, 1932; Murdock, 1934) and also in transmission spectrographs (Du Mond & Bollmann, 1936). In most cases it was explained by a mosaic state of the crystal surfaces (for example James, 1948; Armstrong, 1946). Some of the investigators, however, examined carefully the surfaces of the crystals by the Bragg reflection method and could not find any indication of imperfection. Cork, in particular, pointed out that new theoretical considerations were necessary to explain this phenomenon.

If the intensity enhancement at the margins is due to surface damage, the intensity of the transmitted beam should increase also at the margin nearer to the diffracted beam. Since there is no such enhancement in Fig. 7(*b*) of the previous paper (Kato & Lang, 1959) we may conclude that the intensity enhancement at the margins of the diffracted beam has to be explained by a diffraction effect of a perfect crystal.

4. Experiments of L. C. Brown

In his work* (Brown, 1952) the beam width was rather large (about 1 mm.) but it was collimated well by two perfect calcite crystals. It is of interest to discuss his results here because the character of his incident beam was just complementary to that employed in the intensity profile experiments described in the preceding section.

(A) *Displacement of the transmitted beam*

He measured the position of both edges of the transmitted beam and measured their displacement when the incident beam satisfies the Bragg condition exactly. His results are summarized in Table 1 which is based upon Fig. 11 of the paper (B).

Table 1. *Displacement of edges of transmitted beam*

Thickness t_0 (mm.)	Displacement (mm.) Near side	Far side	Calc.
1·45	0·08	0·03	0·17
2·56	0·3	0·2	0·3

As explained in § 2, when the Bragg condition is satisfied exactly ($y=0$), it is expected that both beam (1) and (2) propagate in a direction of $p=(b-1)/(b+1)$. In his experiments $b\simeq 1$. Therefore the displacement of the edge is estimated as

$$\Delta\xi \simeq t_0 \sin\theta_B \,. \qquad (15)$$

The calculated values are shown in Table 1. The displacement should be the same for both sides of the beam.

Even though the displacement itself is explained qualitatively, agreement between the theoretical and experimental values is not satisfactory. This discrepancy, however, may be explained to some extent as follows. Since the incident beam has a small angular width despite good collimation, some parts of it do not satisfy the Bragg condition exactly. As explained in § 2, these beams flow in a direction nearer either to $\mathbf{K}_0$ or $\mathbf{K}_g$. In thin crystals the transmitted beams which flow to the $\mathbf{K}_0$-side are much stronger than the beams which flow to the $\mathbf{K}_g$-side. Therefore the resultant beam might be expected to be shifted to the $\mathbf{K}_0$-side compared with the case of ideal collimation. With increasing crystal thickness only the (1)-wave can penetrate through the crystal, and it flows in the direction of $p\simeq 0$, so that we can expect that the displacement becomes closer to the theoretical value. This trend is noticed in Brown's experimental results.

(B) *Rocking curve due to a selected beam*

Brown obtained rocking curves due to a selected reflection beam *A* and selected transmission beams *B*, *C*, *D* and *E* which are illustrated in Fig. 5 (Fig. 10 of the paper (B)). His results are shown in Fig. 6 (Fig. 12 of the paper (B)). Due to the geometrical configuration the slit *E* excludes the transmitted beam which flows in a direction $p>0$ and some parts of the beam which flows in a direction $p<0$. Similarly the slit *B* excludes some parts of the beam $p<0$. This means that the effective slit width depends upon

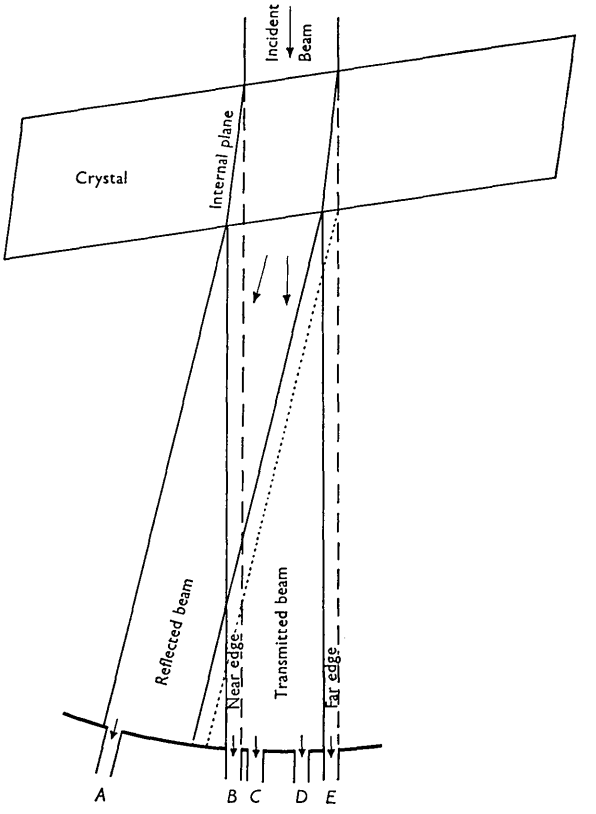

Fig. 5. Geometry of diffracted beams. (Reproduction of Fig. 10 of the paper (*B*)).

* Hereafter we refer to his paper by (B).

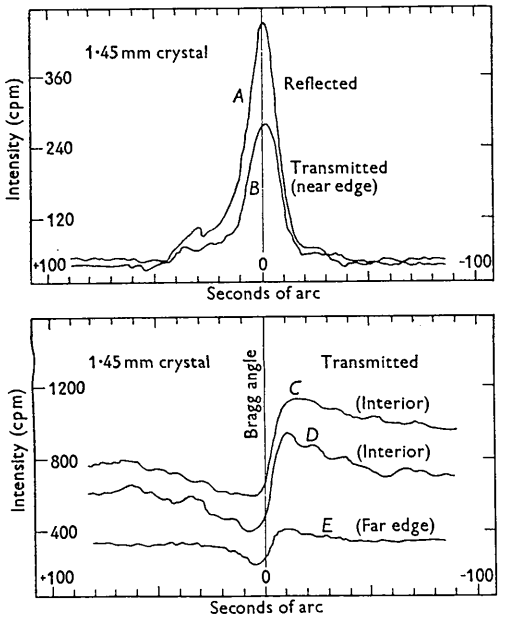

Fig. 6. Rocking curves at various points in beam cross section. (Reproduction of Fig. 12 of the paper (*B*)).

the glancing angle of the incident beam. Thus the rocking curves of the transmitted beam should be expressed as

$$T(y)=|D_0^{(1)}|^2W^{(1)}+|D_0^{(2)}|^2W^{(2)}, \tag{16}$$

where $D^{(i)}$ are given by equation (2) and $W^{(i)}$ are the effective slit widths for the (i)-waves specified as function of parameter y. The slit width can be written on the p-scale as follows, in accord with the experimental conditions

$$\begin{aligned} &\text{Case } B: \quad W^{(i)} = 1 \quad (p>0) \\ &\qquad\qquad\quad\ = 1+p \quad (p<0) \\ &\text{Case } E: \quad W^{(i)} = 0 \quad (p>0) \\ &\qquad\qquad\quad\ = -p \quad (p<0). \end{aligned} \tag{17}$$

Using equations (3) and (7′) $W^{(i)}(y)$ are easily obtained. It is obvious that $W^{(i)}$ are equal to 1 for the cases C and D.

Calculated rocking curves are shown in Fig. 7. In good agreement with Brown's experimental results, the theoretical curve for slit B shows an almost symmetrical peak whose maximum is shifted a little to the smaller-angle side. The rocking curve for slit E has a form similar to the curve for slits C and D, though the peak is flattened so that its maximum value is around half of the maximum value in the C and D cases.

5. Discussion

As explained in the preceding sections, most of the experimental results obtained hitherto can be explained fairly well by the present theory. This kind of study seems to be important from two standpoints: studies of wave dynamics in a perfect crystal and studies on perfectness of real crystals.

Usually studies of wave dynamics in crystals are carried out by measuring the ordinary rocking curves and integrated intensities of reflection. Experiments which are pertinent to energy flow, however, give us another aspect of wave dynamics in crystals. Consider, for example, spatial intensity profile studies. Under reasonable experimental conditions it is not so difficult to measure the intensity profile of a diffracted and a transmitted beam for every increment of 0·1 in p. Relating these to the corresponding y values shows that a spatial line profile study corresponds to a detailed measurement of the central region ($|y|\simeq 0$) of the usual single crystal reflection curve.

If the crystals are different from the ideally perfect state assumed in deriving equation (2), the experimental results should be different from the results expected from the above theory. In ideally mosaic crystals, for example, it is evident that the line profile of the reflected beam has a rectangular form and that of transmitted beams has an appreciable value only in the direction of $\mathbf{K}_0$.

As explained in the introduction, however, the

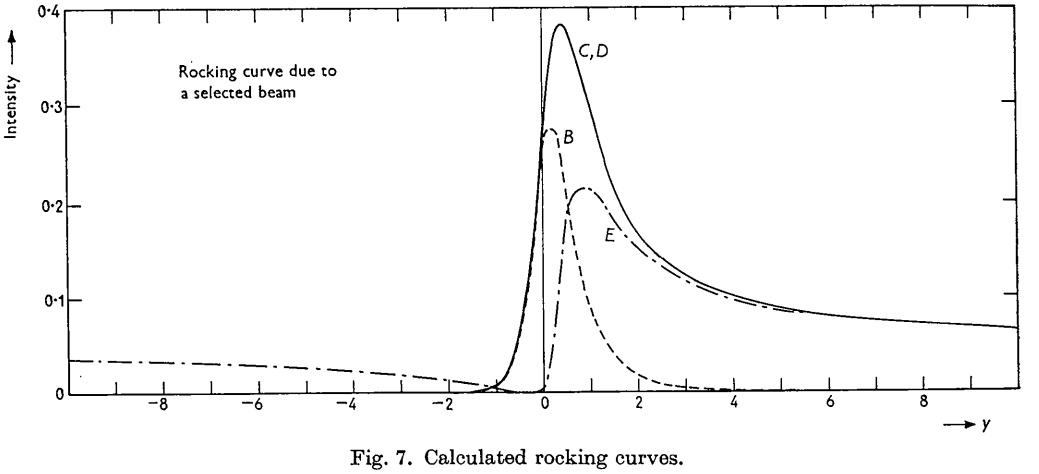

Fig. 7. Calculated rocking curves.

present theory is rather primitive. It seems necessary to develop the theory in such a way that it can be applied to 'Pendellösung' phenomena. In addition it seems desirable to study experimentally the line profiles of reflected and transmitted beams from perfect crystals in more detail, because such a study must show us to what extent the present theory can be applied to the real wave-dynamical situation in crystals.

APPENDIX A

Energy flow in absorbing crystals

In an absorbing crystal, the wave vector $\mathbf{k}_0^{(i)}$ is complex. Since its imaginary part is determined by the real part, wave bundles are constructed through the integration over the dispersion surface determined by the real part of $\mathbf{k}_0^{(i)}$, using the same procedures as in a non-absorbing crystal (Kato, 1952; Ewald, 1958). Moreover, adopting an approximation taking into account the first order effects of $\chi=|\psi_h''|/|\psi_h'|$ in the meaning used in Zachariasen (1945), the real part of $\mathbf{k}_0^{(i)}$ does not change due to absorption. Therefore, the direction of wave bundle propagation must be normal to the dispersion surface determined by the real part of $\mathbf{k}_0^{(i)}$.

The same results are expected also according to Laue's approach to this problem (Laue, 1952, 1953). In an electromagnetic field as well as a material field the real part of a Poynting vector $\mathbf{S}^{(i)}$ and a current vector $\mathbf{J}^{(i)}$ have the meaning of energy flow (cf. for example, Stratton, 1941; Schiff, 1948). As explained above, the real part of $\mathbf{k}_0^{(i)}$ and, accordingly, $\mathbf{k}_g^{(i)}$ are the same for both cases of non-absorbing and absorbing crystals. In addition, the absorption factor of (i)-waves is common for $|D_0^{(i)}|^2$ and $|D_g^{(i)}|^2$ as shown in equation (2). Thus, from equation (1) $\mathbf{S}^{(i)}$ and $\mathbf{J}^{(i)}$ are the same for an absorbing and a non-absorbing crystal, as far as their directions are concerned.

APPENDIX B

Geometrical meaning of $dx/dp\,(\delta p/\delta\xi)$ and $dx/dp\,(\delta p/\delta\eta)$

A crystal wave vector $\mathbf{k}_0$ corresponding to the incident wave vector $\mathbf{K}$ can be expressed as

$$\mathbf{k}_0=\mathbf{K}+\frac{K\delta_0}{\cos(\mathbf{k}_0\mathbf{n}_e)}\mathbf{n}_e \tag{B1}$$

(cf. [3·90] of Zachariasen's text book*) where K is the magnitude of $\mathbf{K}$, $1+\delta_0$ is the refractive index of $\mathbf{k}_0$, $\mathbf{n}_e$ is the inward-drawn normal of the incident surface and $\cos(\mathbf{k}_0, \mathbf{n}_e)$ is the cosine of the angle between $\mathbf{k}_0$ and $\mathbf{n}_e$. The quantity δ_0 can be expressed by

$$\delta_0=\tfrac{1}{2}\{\psi_0-z\pm(z^2+q)^{\frac{1}{2}}\} \tag{B2}$$

according to equation [Z3·121]. As shown in Appendix A, it is sufficient to consider the real part of δ_0 if we are concerned with the direction of energy flow. $\mathbf{K}$ can also be expressed approximately

$$\mathbf{K}\simeq\mathbf{K}_0+(\theta_B-\theta)K\mathbf{x}\,, \tag{B3}$$

where $\mathbf{K}_0$ is the vector $\mathbf{K}$ which satisfies the Bragg condition exactly and $\mathbf{x}$ is a unit vector perpendicular to $\mathbf{K}_0$ in a plane including the $\mathbf{K}_0$ and $\mathbf{g}$ vectors.

Using the relation that a variation of $\mathbf{k}_0$ along the dispersion surface is perpendicular to the corresponding Poynting vector $\mathbf{S}$, we obtain the following relation, by differentiation of equation (B1)

$$\frac{(\mathbf{S}.\mathbf{x})}{\sin 2\theta_B}\frac{\cos(\mathbf{k}_g\mathbf{n}_e)}{\cos(\mathbf{k}_0\mathbf{n}_e)}+\tfrac{1}{2}\frac{(\mathbf{S}.\mathbf{n}_e)}{\cos(\mathbf{k}_0\mathbf{n}_e)}\left\{-1\pm\frac{y}{(1+y^2)^{\frac{1}{2}}}\right\}=0\,. \tag{B4}$$

In deriving this we use relations such as [Z3·116], [Z3·123] and [Z3·141] between θ, y and z. Thus, from equation (3)

$$\mp x=\frac{2\cos(\mathbf{k}_g\mathbf{n}_e)}{\sin 2\theta_B}\frac{(\mathbf{S}.\mathbf{x})}{(\mathbf{S}.\mathbf{n}_e)}-1\,. \tag{B5}$$

From the geometrical relation between $\mathbf{S}$, Θ and ξ as shown in Fig. 2, we get

$$\left|\frac{\delta x}{\delta\xi}\right|=\frac{2\cos(\mathbf{k}_g\mathbf{n}_e)}{\sin 2\theta_B}\frac{\cos(\mathbf{k}_0\mathbf{n}_e)}{\cos^2(\mathbf{S}\mathbf{n}_e)}\frac{d\Theta}{d\xi}\,. \tag{B6}$$

On the other hand we find

$$\frac{t_0\delta\Theta}{\cos(\mathbf{S}\mathbf{n}_e)}=\frac{\cos(\mathbf{S}\mathbf{n}_a)}{\cos(\mathbf{k}_0\mathbf{n}_a)}\delta\xi\,, \tag{B7}$$

where Θ is the angle between $\mathbf{S}$ and the net plane, $\mathbf{n}_a$ is a unit vector perpendicular to the exit surface and t_0 is the distance from the incident surface of a point on the exit surface corresponding to an observation point ξ. Thus finally we obtain

$$\left|\frac{\delta x}{\delta\xi}\right|=\frac{1}{t_o}\frac{\cos(\mathbf{k}_0\mathbf{n}_e)}{\cos(\mathbf{S}\mathbf{n}_e)}\frac{\cos(\mathbf{S}\mathbf{n}_a)}{\cos(\mathbf{k}_0\mathbf{n}_a)}\frac{2\cos(\mathbf{k}_g\mathbf{n}_e)}{\sin 2\theta_B}=\frac{1}{t_o}\frac{2\cos(\mathbf{k}_g\mathbf{n}_e)}{\sin 2\theta_B}\cdot\frac{1}{G_0}\,. \tag{B8a}$$

Similarly, we obtain

$$\left|\frac{\delta x}{\delta\eta}\right|=\frac{1}{t_o}\frac{\cos(\mathbf{k}_0\mathbf{n}_e)}{\cos(\mathbf{S}\mathbf{n}_e)}\frac{\cos(\mathbf{S}\mathbf{n}_a)}{\cos(\mathbf{k}_g\mathbf{n}_a)}\frac{2\cos(\mathbf{k}_g\mathbf{n}_e)}{\sin 2\theta_B}=\frac{1}{t_o}\frac{2\cos(\mathbf{k}_g\mathbf{n}_e)}{\sin 2\theta_B}\cdot\frac{1}{G_g}\,. \tag{B8b}$$

It is a great pleasure for the author to express his sincere thanks to Prof. Ewald for his discussions and particularly for letting him know of Mr Brown's experimental work. Also the author wishes to express

* Hereafter we will cite the equations of his textbook as [Z3·90].

his thanks to Prof. Schwartz who kindly allowed him to reproduce some results of Mr Brown's thesis, and to Prof. Lang for his discussions and encouragement. This work was supported initially by the National Science Foundation and latter by the Office of Naval Research.

References

ARMSTRONG, E. G. (1946). *Bell. Syst. Tech. J.* **25**, 136.
BORRMANN, G. (1950). *Z. Phys.* **127**, 297.
BORRMANN, G., HILDEBRANT, G. & WAGNER, H. (1955). *Z. Phys.* **142**, 406.
BROWN, L. C. (1952). *The Anomalous Transmission of X-rays through Calcite*, M. A. Thesis, Florida State University.
CORK, J. M. (1932). *Phys. Rev.* **42**, 749.
DUMOND, J. & BOLLMANN, V. L. (1936). *Phys. Rev.* **50**, 524.
EWALD, P. P. (1958). *Acta Cryst.* **11**, 888.
JAMES, R. W. (1948). *The Optical Principles and the Diffraction of X-rays*, Chapter 6. London: Bell.
KATO, N. (1952). *J. Phys. Soc. Jap.* **7**, 397.
KATO, N. (1958). *Acta Cryst.* **11**, 885.
KATO, N. (In preparation.)
KATO, N. & LANG, A. R. (1959). *Acta Cryst.* **12**, 787.
KNOWLES, J. W. (1956). *Acta Cryst.* **9**, 61.
LAUE, M. v. (1952). *Acta Cryst.* **5**, 619.
LAUE, M. v. (1953). *Acta Cryst.* **6**, 217.
MURDOCK, C. C. (1934). *Phys. Rev.* **45**, 117.
NIEHRS, H. (1956). *Phys. Verh.* **7**, 212.
SCHIFF, L. I. (1948). *Quantum Mechanics*, p. **24**. New York: McGraw-Hill.
STRATTON, J. A. (1941). *Electromagnetic Theory*, p. 135. New York: McGraw-Hill.
WAGNER, E. H. (1959). *Acta Cryst.* **12**, 345.
ZACHARIASEN, W. H. (1945). *Theory of X-ray Diffraction in Crystals*. New York: Wiley.

Short Communications

Contributions intended for publication under this heading should be expressly so marked; they should not exceed about 500 words; they should be forwarded in the usual way to the appropriate Co-editor; they will be published as speedily as possible; and proofs will not generally be submitted to authors. Publication will be quicker if the contributions are without illustrations.

Acta Cryst. (1960). **13**, 356

Manganese diboride. By IRA BINDER, *Union Carbide Company, White Plains, N. Y.* and BEN POST, *Polytechnic Institute of Brooklyn, Brooklyn, N. Y., U.S.A.*

(*Received* 14 *December* 1959)

Kiessling (1950) investigated the Mn/B system and described a number of manganese borides ranging in composition from Mn_4B to Mn_3B_4. Specimens were prepared by heating mixtures of metal and boron in evacuated silica tubes at 1100–1200 °C. No evidence was found for the existence of MnB_2 or other phases with higher boron content. We have also been unable to prepare the diboride under the conditions described above. However, MnB_2 is formed readily when the reaction temperature is raised to 1400–1500 °C. The product often contains considerable Mn_3B_4 in addition to the diboride. Relatively pure diboride can be prepared conveniently by using 3 to 4 or more parts of boron to one of manganese in the reaction mixture and then removing the excess boron from the product by flotation. No lines due to Mn_3B_4, or other phases, were detected in heavily exposed X-ray diffraction patterns of specimens prepared in this way.

Table 1. *Powder diffraction data*: MnB_2
(Filtered Cu K radiation)

d (Å)	I/I_0	HKL
3·03	25	001
2·60	85	100
1·975	100	101
1·517	8	002
1·503	25	110
1·347	13	111
1·311	15	102
1·302	8	200
1·196	20	201
1·068	18	112
0·984	10	202/210
0·943	10	103
0·936	15	211
0·868	8	300
0·839	5	113
0·834	5	301
0·826	12	212
0·799	10	203

MnB_2 has the AlB_2 type structure; it is isomorphous with TiB_2, VB_2, CrB_2, and other transition metal diborides. The unit cell is hexagonal with $a = 3{\cdot}007$ and $c = 3{\cdot}037$ Å, both $\pm 0{\cdot}002$ Å. Powder diffraction data, obtained with a diffractometer using filtered Cu radiation, are listed in Table 1.

Reference

KIESSLING, R. (1950). *Acta Chem. Scand.* **4**, 146.